Monthly Notices
of the
ROYAL ASTRONOMICAL SOCIETY

MNRAS **469,** S675–S684 (2017)
Advance Access publication 2017 September 28

doi:10.1093/mnras/stx2532

Fluxgate magnetometer offset vector determination by the 3D mirror mode method

F. Plaschke,[1]★ C. Goetz,[2] M. Volwerk,[1] I. Richter,[2] D. Frühauff,[2] Y. Narita,[1] K.-H. Glassmeier[2] and M. K. Dougherty[3]

[1]*Space Research Institute, Austrian Academy of Sciences, Schmiedlstrasse 6, Graz A-8042, Austria*
[2]*Institut für Geophysik und extraterrestrische Physik, Technische Universität Braunschweig, Mendelssohnstrasse 3, D-38106 Braunschweig, Germany*
[3]*The Blackett Laboratory, Imperial College London, London SW7 2BZ, United Kingdom*

Accepted 2017 September 26. Received 2017 August 17; in original form 2017 February 24

ABSTRACT

Fluxgate magnetometers on-board spacecraft need to be regularly calibrated in flight. In low fields, the most important calibration parameters are the three offset vector components, which represent the magnetometer measurements in vanishing ambient magnetic fields. In case of three-axis stabilized spacecraft, a few methods exist to determine offsets: (i) by analysis of Alfvénic fluctuations present in the pristine interplanetary magnetic field, (ii) by rolling the spacecraft around at least two axes, (iii) by cross-calibration against measurements from electron drift instruments or absolute magnetometers, and (iv) by taking measurements in regions of well-known magnetic fields, e.g. cometary diamagnetic cavities. In this paper, we introduce a fifth option, the 3-dimensional (3D) mirror mode method, by which 3D offset vectors can be determined using magnetic field measurements of highly compressional waves, e.g. mirror modes in the Earth's magnetosheath. We test the method by applying it to magnetic field data measured by the following: the *Time History of Events and Macroscale Interactions during Substorms-C* spacecraft in the terrestrial magnetosheath, the *Cassini* spacecraft in the Jovian magnetosheath and the *Rosetta* spacecraft in the vicinity of comet 67P/Churyumov–Gerasimenko. The tests reveal that the achievable offset accuracies depend on the ambient magnetic field strength (lower strength meaning higher accuracy), on the length of the underlying data interval (more data meaning higher accuracy) and on the stability of the offset that is to be determined.

Key words: magnetic fields – plasmas – waves – space vehicles: instruments.

1 INTRODUCTION

The characterization of the plasma environment around the Sun, Sun-orbiting planets, their moons, as well as comets traversing the Solar system, requires *in situ* measurements of the magnetic field. These measurements are often performed by spacecraft-attached fluxgate magnetometers, because they can be designed to be small, lightweight, robust, yet stable with regard to their calibration parameters (e.g. Acuña 2002; Glassmeier et al. 2007a,b; Auster et al. 2008; Russell et al. 2016). The raw output of these magnetometers $\boldsymbol{B}_{\rm raw}$ needs to be converted to magnetic field vectors $\boldsymbol{B}$ in meaningful units and coordinate systems by applying a calibration matrix $\mathbf{M}$ and an offset vector $\boldsymbol{O}$ in the following manner (e.g. Kepko et al. 1996; Plaschke et al. 2014):

$$\boldsymbol{B} = \mathbf{M} \cdot \boldsymbol{B}_{\rm raw} - \boldsymbol{O}. \quad (1)$$

The calibration matrix applies gain factors to the outputs of a three-dimensional (3D) fluxgate magnetometer sensor. Furthermore, $\mathbf{M}$ includes an orthogonalization matrix determined by six angles that define the sensor axes' directions with respect to the spacecraft. That matrix transforms the gain-corrected sensor output into an orthogonal, spacecraft-fixed coordinate system. In total, nine parameters (three gains and six angles) contribute to $\mathbf{M}$.

The 3D offset vector $\boldsymbol{O}$ represents the magnetometer output in zero ambient field. It will contain any sensor or electronics (i.e. instrument) related offset contributions, but also, most notably, the fields that are generated by the spacecraft at the position of the magnetometer sensor. The offset components are known to be more time-varying than the gains and angles constituting $\mathbf{M}$. In the case of the *Cluster* spacecraft (Balogh et al. 2001), long (medium-term) offset variations of the order of a few tenths of a nanotesla per year (peak-to-peak) were reported by Alconcel et al. (2014). These variations can be much larger if the considered spacecraft are not as magnetically clean as *Cluster*. Hence, the offset vector needs to be regularly updated in flight.

★ E-mail: ferdinand.plaschke@oeaw.ac.at

© 2017 The Authors
Published by Oxford University Press on behalf of the Royal Astronomical Society

Downloaded from https://academic.oup.com/mnras/article-abstract/469/Suppl_2/S675/4265357
by guest
on 13 November 2017

The spin-stabilization of spacecraft greatly supports the determination of the spin plane components of $\boldsymbol{O}$. If those components are not correctly chosen, then the spin plane magnitude of $\boldsymbol{B}$ will feature a noticeable spin tone. The spin-axis component of $\boldsymbol{O}$ is less easy to obtain. It can be determined by analysing Alfvénic fluctuations of the interplanetary magnetic field (IMF), present in the pristine solar wind (e.g. Belcher 1973; Hedgecock 1975; Leinweber et al. 2008). Thereby, it is assumed that the magnetic field magnitude remains unchanged. Furthermore, it is possible to use suitable measurements by other instruments, e.g. electron gyro-time data from electron drift instruments (Russell et al. 2016; Torbert et al. 2016) or magnetic field magnitude data from an absolute magnetometer, to cross-calibrate the offset against (see Georgescu et al. 2006; Nakamura et al. 2014; Plaschke et al. 2014). When neither data from those additional instruments nor IMF measurements are available, then magnetic field observations of mirror modes may be used to compute the spin-axis offset (Plaschke & Narita 2016), by using the mirror mode method.

Mirror modes are highly compressional waves with large $\Delta B/B$ ratios ($B = |\boldsymbol{B}|$) that arise, for instance, in the Earth's dayside magnetosheath behind the quasi-perpendicular bow shock, where the shocked ions have a strong temperature asymmetry $T_\perp > T_\parallel$. The instability criterion is given by

$$1 + \beta_\perp \left(1 - \frac{T_\perp}{T_\parallel}\right) < 0, \tag{2}$$

(see e.g. Hasegawa 1969; Tsurutani et al. 1982; Glassmeier et al. 1993; Baumjohann et al. 1999; Lucek et al. 1999; Constantinescu et al. 2003). The instability criterion is the same for ion cyclotron waves, which normally will have a greater growth rate (Gary, Fuselier & Anderson 1993). However, the growth of ion cyclotron waves may be inhibited by plasma inhomogeneities created by mirror modes, as proposed by Southwood & Kivelson (1993). Furthermore, their growth is inhibited by the presence of helium ions (Gary et al. 1993). In general, lower plasma-β conditions are propitious for the appearance of ion cyclotron waves, while higher plasma-β conditions favour the generation of mirror modes (e.g. Schwartz, Burgess & Moses 1996). The mirror mode structures resemble magnetic bottles of lower/higher magnetic fields and anticorrelated higher/lower densities that are convected with the shocked solar wind plasma within the magnetosheath in antisunward direction.

The 1D mirror mode method (Plaschke & Narita 2016) makes use of the fact that the magnetic field variations corresponding to mirror modes are strongest in the magnitude of $\boldsymbol{B}$, while the direction of the magnetic field remains approximately constant (e.g. Price, Swift & Lee 1986; Tsurutani et al. 2011). Hence, any systematic deviations in magnetic field direction with respect to the direction of maximum variance along the spin axis can be interpreted to result from a remaining, not yet corrected spin-axis offset.

It is important to note that strong $\Delta B/B$ ratios without $\boldsymbol{B}$ direction changes are not unique to mirror modes: Observations of any other highly compressional waves and fluctuations are suitable for offset determination with the mirror mode method.

The mirror mode method has been successfully applied to data of the five *Time History of Events and Macroscale Interactions during Substorms* (*THEMIS*) spacecraft (Angelopoulos 2008). The apogee distances of the three inner spacecraft (*THEMIS-A*, *-D* and *-E*) are too low to reach the pristine solar wind under normal (not extreme) circumstances. They are high enough, though, for the spacecraft to regularly enter the dayside magnetosheath within a few months per year. Hence, it was possible to determine and correct the spin-axis offsets retroactively with the mirror mode method (Frühauff, Plaschke & Glassmeier 2017). The mirror mode method as introduced in Plaschke & Narita (2016) could be applied, because the *THEMIS* spacecraft are spin-stabilized, but it does not work for three-axis stabilized spacecraft.

Here, we introduce the 3D mirror mode method for three-axis stabilized spacecraft. Though based on the same principles, it is not an enhanced version of the method detailed in Plaschke & Narita (2016), but a new development. The method is then tested by applying it to well-calibrated *THEMIS-C* (Angelopoulos 2008; Auster et al. 2008) and *Cassini* (André, Erdös & Dougherty 2002; Dougherty et al. 2004) magnetometer data from the Earth's and Jupiter's magnetosheath regions, respectively. Finally, we apply the method to *Rosetta* magnetometer data (Glassmeier et al. 2007a), whose calibration is significantly more challenging than that of the *THEMIS* and *Cassini* spacecraft.

2 3D MIRROR MODE METHOD

In accordance with the mirror mode method (Plaschke & Narita 2016), we shall start with a time series of magnetic field measurements that contain strongly compressional fluctuations, either from mirror modes or other compressional waves. The magnetic field measurements $\boldsymbol{B}$ shall be well-calibrated but for the offset vector $\boldsymbol{O}$. Offset corrected data $\boldsymbol{B}_{\rm corr}$ are obtained via

$$\boldsymbol{B}_{\rm corr} = \boldsymbol{B} - \boldsymbol{O}. \tag{3}$$

The time series are divided into shorter subintervals of length $t_{\rm int}$. For each of the subintervals, the maximum variance direction $\boldsymbol{D}$ with $|\boldsymbol{D}| = 1$ is computed. This is the eigenvector of the covariance matrix of the magnetic field measurements corresponding to the largest eigenvalue λ_1 (Sonnerup & Cahill 1967). In the presence of highly compressional waves, systematic differences in direction between $\boldsymbol{B}$ averages over any subinterval (denoted with $\boldsymbol{B}^{\rm a}$) and the corresponding $\boldsymbol{D}$ may be attributed to a non-vanishing offset $\boldsymbol{O}$.

The direction of $\boldsymbol{B}^{\rm a}$ should be most sensitive to offset components perpendicular to $\boldsymbol{D}$. Correspondingly, each subinterval just yields an estimate of the offset component along $\boldsymbol{e}$, perpendicular to $\boldsymbol{D}$ in the plane defined by $\boldsymbol{B}^{\rm a}$ and $\boldsymbol{D}$:

$$\boldsymbol{e} = \frac{\boldsymbol{B}^{\rm a} - (\boldsymbol{B}^{\rm a} \cdot \boldsymbol{D})\boldsymbol{D}}{|\boldsymbol{B}^{\rm a} - (\boldsymbol{B}^{\rm a} \cdot \boldsymbol{D})\boldsymbol{D}|}. \tag{4}$$

The offset in that direction is $\boldsymbol{e} \cdot \boldsymbol{O}$, which should ideally coincide with $O_B = \boldsymbol{e} \cdot \boldsymbol{B}^{\rm a}$. The vector $\boldsymbol{O}$ may now be computed by minimizing the difference between $\boldsymbol{e} \cdot \boldsymbol{O}$ and O_B over all subintervals as follows:

$$\sum_i \left(\frac{\boldsymbol{e}_i \cdot \boldsymbol{O} - O_{Bi}}{\Delta O_{Bi}}\right)^2 = \min. \tag{5}$$

Here, the subintervals are indexed by i. The uncertainty values ΔO_{Bi} may be used to weigh the contributing subintervals differently. They may be set to $\Delta O_{Bi} = \Delta D_i$ with

$$\Delta D_i = \arctan(\sqrt{\lambda_{2i}/\lambda_{1i}}). \tag{6}$$

Here, ΔD_i are the angular uncertainties in $\boldsymbol{D}_i$, which should dominate by far over those in $\boldsymbol{B}_i^{\rm a}$ as shown in Plaschke & Narita (2016). The quotient $\lambda_{2i}/\lambda_{1i}$ is the ratio of intermediate to largest eigenvalues corresponding to the maximum variance analysis performed with the data of subinterval i. Equation (5) is equivalent to

$$\boldsymbol{O} = \mathbf{A}^{-1} \cdot \boldsymbol{d} \tag{7}$$

Downloaded from https://academic.oup.com/mnras/article-abstract/469/Suppl_2/S675/4265357
by guest
on 13 November 2017

with

$$A_{ab} = \sum_i \frac{e_{ia} e_{ib}}{\Delta O_{Bi}^2} \tag{8}$$

and

$$d_a = \sum_i \frac{e_{ia} O_{Bi}}{\Delta O_{Bi}^2}. \tag{9}$$

Equations (7), (8) and (9) are obtained by calculating the derivatives of equation (5) with respect to the three components of $\boldsymbol{O}$.

A key element is the selection of subintervals contributing to the above mentioned sums. Only those intervals containing highly compressible waves/fluctuations, yielding good estimates of $\boldsymbol{D}_i$ shall be used. The compressibility of waves is expressed in the ratio $\Delta B_i / B_i^{\mathrm{a}}$. However, due to an expected non-vanishing offset $\boldsymbol{O}$, $B_i^{\mathrm{a}} = |\boldsymbol{B}_i^{\mathrm{a}}|$ may not be correct. Thus, we require just ΔB_i as defined below to surpass a certain threshold $C_{\Delta B}$:

$$\Delta B_i = \max(\boldsymbol{B}_i \cdot \boldsymbol{D}_i) - \min(\boldsymbol{B}_i \cdot \boldsymbol{D}_i) > C_{\Delta B}, \tag{10}$$

and $\boldsymbol{B}_i^{\mathrm{a}}$ and $\boldsymbol{D}_i$ to be roughly aligned:

$$\alpha_i = \arccos\left(\frac{\boldsymbol{B}_i^{\mathrm{a}} \cdot \boldsymbol{D}_i}{|\boldsymbol{B}_i^{\mathrm{a}}|}\right) < C_\alpha. \tag{11}$$

Note that $\boldsymbol{B}_i$ represents a time series of magnetic field vectors pertaining to interval i, whereas there is only one maximum variance vector $\boldsymbol{D}_i$ associated with that interval. Here, α_i is the angle between the average magnetic field direction and the maximum variance direction pertaining to interval i. Furthermore, we require the direction of $\boldsymbol{D}_i$ to be well-defined by setting a low threshold on ΔD_i (see equation 6):

$$\Delta D_i < C_{\Delta D}. \tag{12}$$

ΔB_i and ΔD_i are independent of $\boldsymbol{O}$. Note, however, that the angles α_i change if an offset correction $\boldsymbol{O}$ is applied. Thus, equation (7) is only able to yield an estimate for the offset vector $\boldsymbol{O}$ to be subtracted from the magnetic field vectors $\boldsymbol{B}$ (see equation 3): $\boldsymbol{O}$ needs to be refined iteratively.

Hence, in summary, the 3D mirror mode method is applied as follows: (i) A time series of magnetic field data (vectors $\boldsymbol{B}$) containing highly compressional waves is divided into subintervals. (ii) A subset of those subintervals is selected by applying equations (10), (11) and (12). (iii) Then, an offset estimate $\boldsymbol{O}$ is computed via equation (7), using only data from the selected subintervals. (iv) All magnetic field vectors are corrected with that offset estimate via equation (3). The corrected data $\boldsymbol{B}_{\mathrm{corr}}$ becomes $\boldsymbol{B}$ and the steps (i to iv) are repeated until the offset correction $|\boldsymbol{O}|$ becomes smaller than a threshold C_O. The final offset $\boldsymbol{O}_{\mathrm{f}}$ is the sum of the offset estimates obtained over all iterations:

$$\boldsymbol{O}_{\mathrm{f}} = \sum_n \boldsymbol{O}_n, \tag{13}$$

here, n is the index pertaining to the iterations. Note that it may be necessary to apply a step size control for the iterative process to converge: in step (iv) not the entire offset estimate $\boldsymbol{O}$ may be applied to $\boldsymbol{B}$, but only a fraction $1/S$ of $\boldsymbol{O}$. Larger values of S make the iterative process more stable, but also more slowly converging.

3 APPLICATION TO *THEMIS*

We apply the 3D mirror mode method to one month of *THEMIS-C* fluxgate magnetometer (Auster et al. 2008) observations in the Earth's dayside magnetosheath from 2008 July to test the accuracy of the method. This data set has already been used in Plaschke & Narita (2016). Hence, we can compare the results of the 3D and previously introduced 1D mirror mode methods.

The data set is comprised of spin resolution data (∼3 s sampling period). Corresponding position data and ion density moments measured by the electrostatic analyzer (McFadden et al. 2008) are also loaded to automatically identify intervals during which the spacecraft was present in the magnetosheath: The spacecraft shall be at a distance of over $8\,R_{\mathrm{E}}$ (Earth radii) from the Earth's centre and shall measure ion densities larger than twice the solar wind ion density, as given in NASA's OMNI high resolution solar wind data set (King & Papitashvili 2005). The latter criterion was successfully used e.g. in Plaschke, Hietala & Angelopoulos (2013) for the automatic selection of dayside magnetosheath intervals. Note that the position and plasma data are not needed if those intervals are selected manually. In total, 143 h of magnetosheath data are selected, that is 4.6 h of magnetosheath dwell time per day on average. The data are transformed into the despun sun-sensor L-vector (DSL) coordinate system, which is inertial and aligned along the z-direction with the spacecraft spin axis.

Fig. 1 shows an example interval of *THEMIS-C* data, taken on 2008 July 6. *THEMIS-C* was on an outbound orbit and entered the magnetosheath from the inner magnetosphere shortly after 12:00 UT. This is visible in the magnetic field data ($\boldsymbol{B}$ in DSL depicted in panel a). Correspondingly, the density measured by *THEMIS-C* surpassed twice the solar wind values given by the OMNI data set (see panel b). Before 16:00 UT, *THEMIS-C* entered the solar wind, which is associated with a drop in density and magnetic field magnitude.

It may seem surprising that we test a method specifically designed for three-axis stabilized spacecraft using data from *THEMIS-C*, which is a spin-stabilized spacecraft. The reason is that the spin stabilization allows for a perfect offset compensation in the two spin plane components (x and y in DSL) of the spin resolution data (Auster et al. 2008). Furthermore, the spin-axis offset has been determined and corrected by analysis of IMF Alfvénic fluctuations with uncertainties on the order of a few tenths of a nanotesla (Leinweber et al. 2008). Spacecraft influences on the offsets are anyway limited, as the flux-gate magnetometer sensor is separated from the spacecraft main body by a 2 m long boom (Auster et al. 2008).

Hence, the despun *THEMIS-C* data mimic magnetic field measurements from a three-axis stabilized spacecraft that are very well corrected with respect to the offset. The 3D mirror mode method should ideally determine $\boldsymbol{O}_{\mathrm{f}}$ to be zero in x and y, and close to zero in z. By applying the 1D mirror mode method to the entire month of magnetosheath data, Plaschke & Narita (2016) found $O_{z\mathrm{f}} = 0.21$ nT as residual z-axis offset.

Following Plaschke & Narita (2016), we divide the magnetosheath data into $t_{\mathrm{int}} = 3$ min long intervals, shifted by $t_{\mathrm{shift}} = 10$ s. Therewith, we obtain 47 831 intervals without data gaps. In Fig. 1 panels (c) and (d), the average magnetic fields $\boldsymbol{B}^{\mathrm{a}}$ and maximum variance directions $\boldsymbol{D}$ are shown for the 2008 July 6 *THEMIS-C* magnetosheath traversal.

Depending on the choice of $C_{\Delta B}$ and $C_{\Delta D}$, more or less intervals will be considered for the offset computation. Larger $C_{\Delta B}$ and lower $C_{\Delta D}$ will increase the quality of the selected intervals while decreasing the sample size. Good statistics, however, are necessary for the method to perform well, as individual vectors $\boldsymbol{B}^{\mathrm{a}}$ and $\boldsymbol{D}$ may easily deviate by 20° even for strongly compressional mirror mode intervals (see Erdős & Balogh 1996; Enríquez-Rivera et al. 2013; Schmid et al. 2014). The corresponding offset errors are averaged out when using a larger sample size of intervals.

Downloaded from https://academic.oup.com/mnras/article-abstract/469/Suppl_2/S675/4265357
by guest
on 13 November 2017

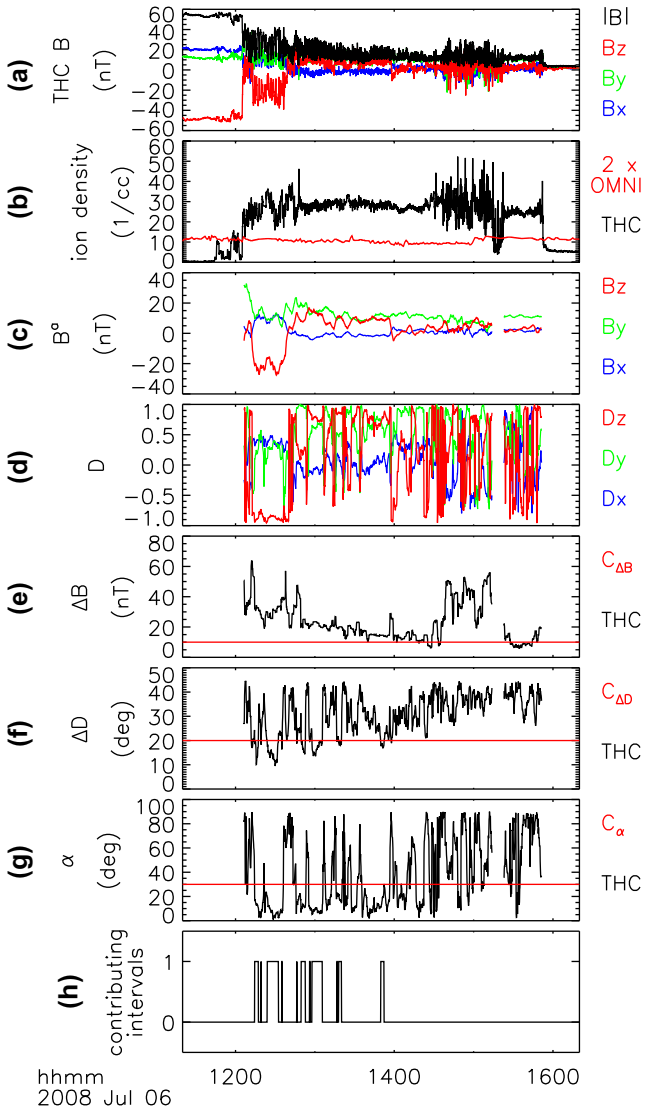


Figure 1. From the top to bottom: (a) *THEMIS-C* magnetic field data $\boldsymbol{B}$ in DSL, (b) *THEMIS-C* ion density (black) and twice the solar wind density given by the OMNI data set (red), (c) subinterval averages $\boldsymbol{B}^{\mathrm{a}}$ in DSL, (d) maximum variance direction $\boldsymbol{D}$ in DSL, (e) field changes in that direction ΔB (black) and $C_{\Delta B} = 10\,\mathrm{nT}$ (red), (f) angular uncertainties ΔD with respect to $\boldsymbol{D}$ (black) and $C_{\Delta D} = 20^\circ$ (red), (g) angle between $\boldsymbol{D}$ and $\boldsymbol{B}^{\mathrm{a}}$ (black) and $C_\alpha = 30^\circ$ (red), and (h) a flag to identify the selected subintervals which fulfil all criteria and, hence, contribute to offset determination.

Fig. 2 shows ΔD as a function of ΔB for all 47 831 subintervals. As can be seen, ΔB values along the maximum variance directions (equation 10) range from a few to over 100 nT. ΔD is constrained between 7° and 45°. The median values of ΔD and ΔB are 32.5° and 16.6 nT, respectively. As ΔD represents the angular error in $\boldsymbol{D}$, a low, single digit value would be desirable for the threshold value $C_{\Delta D}$. This is not possible, because none of the subintervals would fulfil such a criterion. As a compromise, we choose $C_{\Delta D} = 20^\circ$, based on Fig. 2. To avoid restricting our sample size further, we choose $C_{\Delta B} = 10\,\mathrm{nT}$, which already corresponds to quite strong fluctuations considering the median $B^{\mathrm{a}} = 14\,\mathrm{nT}$ over all subintervals. $C_{\Delta B}$ and $C_{\Delta D}$ are depicted by red lines in Fig. 2. They enclose 4640 crosses in the lower right-hand corner of the figure pertaining to as many subintervals that are further considered for offset determination.

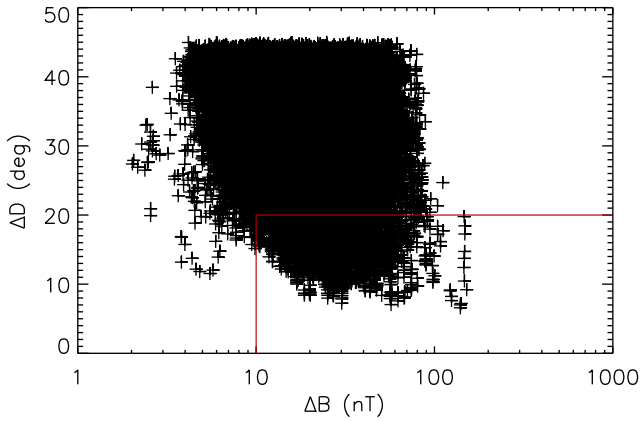


Figure 2. ΔD over ΔB pertaining to 47 831 magnetosheath subintervals of *THEMIS-C* data from 2008 July. The red lines depict the 10 nT and 20° levels, respectively.

In Fig. 1, ΔB and ΔD as well as the respective thresholds $C_{\Delta B}$ and $C_{\Delta D}$ are shown in panels (e) and (f). We see there too that the criterion on ΔB is very permissive, while our choice of $C_{\Delta D}$ is rather strict. Only between 12:00 and 14:00 UT, $\Delta D < C_{\Delta D}$ is sometimes fulfilled.

The number of subintervals is further reduced by C_α, which we set to 30° following Plaschke & Narita (2016). For the 2008 July 6 *THEMIS-C* magnetosheath traversal, the angles α and C_α are shown in panel (g) of Fig. 1. The last panel (h) of that figure flags all subintervals for which the criteria with respect to ΔB, ΔD and α are fulfilled. Hence, those contribute to the first round of the iterative offset determination.

With $C_O = 10\,\mathrm{pT}$ and $S = 10$ controlling that iterative offset determination process, we obtain

$$\boldsymbol{O}_{\mathrm{f}} = (-0.23,\ 0.82,\ -0.17)\,\mathrm{nT} \tag{14}$$

after 24 iterations. The initial number of subintervals used, due to applying C_α, is 2505; at the final step, 2511 intervals contribute. Hence, $C_\alpha = 30^\circ$ reduces the number of subintervals in this case by about 46 per cent with respect to the 4640 subintervals initially selected by applying the thresholds $C_{\Delta B}$ and $C_{\Delta D}$.

As can be seen, all final offset components are below 1 nT, the expected values are zero; the magnitude of $\boldsymbol{O}_{\mathrm{f}}$ is 0.87 nT. This indicates that given a sufficient amount of data, offset vector accuracies on the order of or below 1 nT can be achieved with the 3D mirror mode method. Hence, the achievable accuracy seems to be about one order of magnitude lower than that of the 1D mirror mode method. Note that a decrease in accuracy is expected due to the two additional degrees of freedom.

Next, we add artificial offset vectors $\boldsymbol{O}_{\mathrm{add}}$ to the *THEMIS* data to see if the 3D mirror mode method is able to recover those offsets (final offset values $\boldsymbol{O}_{\mathrm{rec}}$). The results are summarized in Table 1. The two left-hand columns show the added and recovered offset vectors. The difference between these two is given in the right-hand column; it should and, indeed, does coincide with the result from the application of the 3D mirror mode method to the unaltered *THEMIS* data, shown in equation (14). Hence, the method is able to correctly determine non-zero offset vectors with the same precision.

We investigate how many subintervals need to contribute to the offset determination so that a certain level of accuracy is reached. Therefore, we preselect the 4640 subintervals for which $\Delta B > C_{\Delta B} = 10\,\mathrm{nT}$ and $\Delta D < C_{\Delta D} = 20^\circ$ is fulfilled. We then calculate offsets $\boldsymbol{O}_{\mathrm{f}}$ with all possible combinations of 500, 1000 and 2000

Downloaded from https://academic.oup.com/mnras/article-abstract/469/Suppl_2/S675/4265357
by guest
on 13 November 2017

Table 1. Left column: offset vectors $\boldsymbol{O}_{\rm add}$ added to *THEMIS* data. Middle column: offset vectors $\boldsymbol{O}_{\rm rec}$ recovered by the mirror mode method. Right column: $\boldsymbol{O}_{\rm rec} - \boldsymbol{O}_{\rm add}$, which should ideally coincide with the result shown in equation (14).

$\boldsymbol{O}_{\rm add}$ [nT]	$\boldsymbol{O}_{\rm rec}$ [nT]	$\boldsymbol{O}_{\rm rec} - \boldsymbol{O}_{\rm add}$ [nT]
(5, 0, 0)	(4.76, 0.82, −0.17)	(−0.24, 0.82, −0.17)
(0, 5, 0)	(−0.23, 5.82, −0.17)	(−0.23, 0.82, −0.17)
(0, 0, 5)	(−0.24, 0.82, 4.83)	(−0.24, 0.82, −0.17)
(5, 5, 0)	(4.76, 5.82, −0.17)	(−0.24, 0.82, −0.17)
(5, 0, 5)	(4.76, 0.82, 4.83)	(−0.24, 0.82, −0.17)
(0, 5, 5)	(−0.24, 5.82, 4.83)	(−0.24, 0.82, −0.17)
(5, 5, 5)	(4.76, 5.82, 4.83)	(−0.24, 0.82, −0.17)

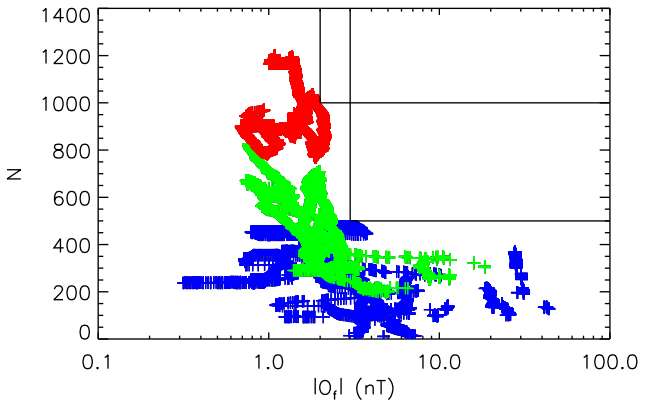


Figure 3. Number of subintervals N fulfilling also $\alpha < C_\alpha = 30^\circ$ from selections of 500 (blue), 1000 (green) and 2000 (red) subsequent subintervals that also fulfil $\Delta D < C_{\Delta D} = 20^\circ$ and $\Delta B > C_{\Delta B} = 10$ nT as a function of the corresponding final offset accuracy $|\boldsymbol{O}_{\rm f}|$. Vertical lines depict $|\boldsymbol{O}_{\rm f}| = 2$ nT and 3 nT; horizonal lines $N = 500$ and 1000, respectively.

subsequent subintervals thereof. Only a subset of N of those 500, 1000 and 2000 subintervals will be used for which $\alpha < C_\alpha = 30^\circ$ is also fulfilled. Fig. 3 shows this number N as a function of the accuracy of the offset determination $|\boldsymbol{O}_{\rm f}|$. Blue, green and red crosses correspond to selections of 500, 1000 and 2000 subintervals, respectively. As can be seen, there is a correlation between N and $|\boldsymbol{O}_{\rm f}|$: higher N are generally associated with smaller $|\boldsymbol{O}_{\rm f}|$, i.e. more accurate offset determinations. The lines in the figure indicate that all $|\boldsymbol{O}_{\rm f}|$ are smaller than 3 nT (2 nT) if more than $N = 500$ (1000) subintervals contribute.

$N = 500$ (1000) means that roughly twice as many subintervals are needed that fulfil $\Delta B > C_{\Delta B}$ and $\Delta D < C_{\Delta D}$, i.e. 1000 (2000). As those are selected from about 10 times as many subintervals of magnetosheath data, 10000 (20000) of those are required to achieve offset accuracies of 3 nT (2 nT). With $t_{\rm shift} = 10$ s, these numbers convert to 1×10^5 s (2×10^5 s), i.e. approximately 28 h (56 h) of magnetosheath data.

4 APPLICATION TO *CASSINI*

To test the method against data from a three-axis stabilized spacecraft, we use magnetic field data from the *Cassini* flux-gate magnetometer (Dougherty et al. 2004). In particular, we use data from a Jupiter flyby that took place in early 2001 (Matson, Spilker & Lebreton 2002), during which *Cassini* traversed the dusk flank of the Jovian magnetosheath. Therein, *Cassini* observed mirror mode activity over an extended period of time (André et al. 2002).

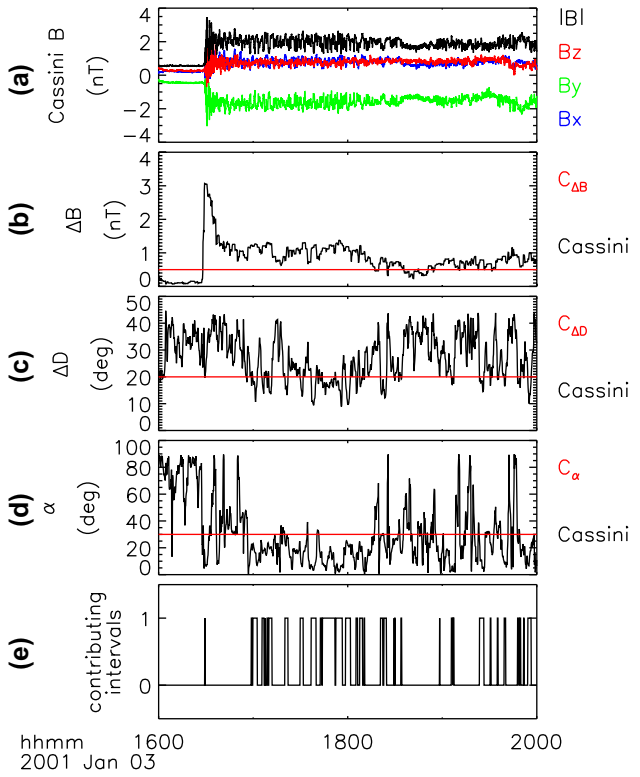


Figure 4. From the top to bottom: (a) *Cassini* magnetic field data $\boldsymbol{B}$ in spacecraft coordinates, (b) field changes ΔB in maximum variance directions (black) and $C_{\Delta B} = 0.5$ nT (red), (c) angular uncertainties ΔD with respect to $\boldsymbol{D}$ (black) and $C_{\Delta D} = 20^\circ$ (red), (d) angle between $\boldsymbol{D}$ and $\boldsymbol{B}^{\rm a}$ (black) and $C_\alpha = 30^\circ$ (red), and (e) a flag to identify the selected subintervals that fulfil all criteria and, hence, contribute to offset determination (first iteration).

Data are available between 2001 January 3–22 and from 2001 February 16, 00:05 UT, to 2001 February 18, 08:23 UT. Excluding data gaps, this amounts to 192 h of magnetic field measurements, almost exclusively from the Jovian magnetosheath. The data are calibrated and the offsets have already been corrected by making use of Alfvénic fluctuations in the solar wind and spacecraft rolls. Spacecraft influences on the magnetometer offsets are anyway limited in the *Cassini* case, as the flux-gate magnetometer is mounted on a long boom at a distance of approximately 5.5 m from the spacecraft main body (Dougherty et al. 2004). The data we use are given in spacecraft coordinates, wherein any residual offset vectors due to spacecraft fields should be fixed. As in the *THEMIS* case, we expect offsets obtained with the 3D mirror mode method to vanish. The data are, again, divided into $t_{\rm int} = 3$ min long subintervals, shifted by $t_{\rm shift} = 10$ s, yielding 68 755 subintervals without data gaps.

Data pertaining to 2001 January 3, 16:00 to 20:00 UT, are shown exemplarily in Fig. 4. Panel (a) of that figure shows the magnetic field data from a Jovian bow shock passage (jump in magnetic field). Right after *Cassini* enters the magnetosheath, compressional wave activity is observed. By comparing panels (a) of Figs 1 and 4, it becomes apparent that the field strength in the Jovian magnetosheath is much smaller than in the terrestrial magnetosheath, by about a factor of 10. Hence, the changes in field ΔB in maximum variance direction are also much smaller.

This can also be seen in Fig. 5, which shows ΔD against ΔB (see also panels b and c of Fig. 4). Median ΔD and ΔB are 26.7° and 0.34 nT, respectively. Correspondingly, we adjust $C_{\Delta B} = 0.5$ nT but keep $C_{\Delta D} = 20^\circ$ with respect to the *THEMIS* case. By applying

Downloaded from https://academic.oup.com/mnras/article-abstract/469/Suppl_2/S675/4265357
by guest
on 13 November 2017

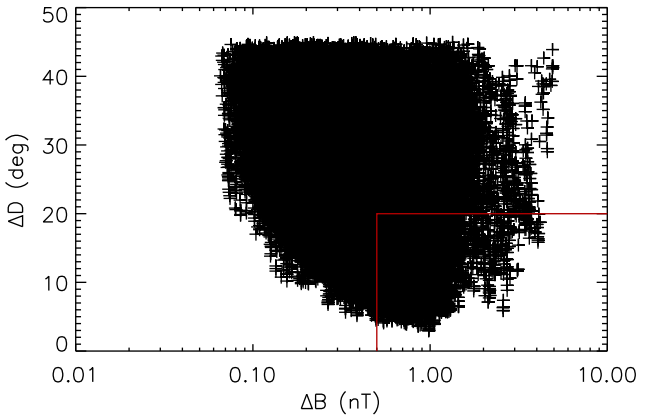


Figure 5. ΔD over ΔB pertaining to 68 755 subintervals of *Cassini* data from 2001 January 3 to February 18. The red lines depict the 0.5 nT and 20° levels, respectively.

these criteria, 8852 subintervals remain for offset determination, almost twice as many as resulting from one month of *THEMIS-C* measurements. Furthermore, we set $C_\alpha = 30°$ (panel d of Fig. 4), $C_O = 10\,\mathrm{pT}$ and $S = 10$. Therewith, we obtain an offset vector:

$$\boldsymbol{O}_\mathrm{f} = (0.05, 0.03, 0.11)\,\mathrm{nT} \tag{15}$$

after 18 iterations. Our choice of C_α initially restricts the amount of subintervals contributing to the offset to 5586; this number slightly increases to 5592 at the end of the computations.

The offset vector is very small: $|\boldsymbol{O}_\mathrm{f}| = 0.12\,\mathrm{nT}$, much smaller than in the *THEMIS* case. Accordingly, the achievable accuracy is much larger. This fact may partly be explained by the higher number of subintervals contributing to the offset (see previous section). Another reason, however, is clearly the much smaller background field in the Jovian magnetosheath: Individual offset estimates $O_B = \boldsymbol{e} \cdot \boldsymbol{B}^\mathrm{a}$ are determined for each subinterval; those are then used to compute one offset vector per iteration via equations (5) or (7). Hence, angular uncertainties in $\boldsymbol{e}$ yield uncertainties of O_B and, ultimately, of $\boldsymbol{O}_\mathrm{f}$ that are proportional to $\boldsymbol{B}^\mathrm{a}$. This knowledge leads to an ansatz of the form

$$\Delta O_\mathrm{f} = c \frac{\sum_i |\boldsymbol{B}_i^\mathrm{a}|/N}{\sqrt{N}} \tag{16}$$

for the uncertainty ΔO_f of the final offset $\boldsymbol{O}_\mathrm{f}$. Here, $\sum_i |\boldsymbol{B}_i^\mathrm{a}|/N$ is the average of the mean fields $|\boldsymbol{B}_i^\mathrm{a}|$ of all N contributing subintervals in the final iteration step of the application of the 3D mirror mode method. As in Plaschke & Narita (2016), we assume ΔO_f to be proportional to $1/\sqrt{N}$, as O_f is the result of an averaging process. The constant c is a unitless factor.

With the result $|\boldsymbol{O}_\mathrm{f}| = 0.12\,\mathrm{nT}$ obtained in this section (equation 15), we are able to compute c. The corresponding N and $\sum_i |\boldsymbol{B}_i^\mathrm{a}|/N$ are 5592 and 1.35 nT, respectively. These numbers yield

$$c = 6.57. \tag{17}$$

This number should be regarded as spacecraft specific, as it should be dependent on influences other than $|\boldsymbol{B}^\mathrm{a}|$ and N to the accuracy of the offset determination process. For instance, c should be dependent on the amplitude of true short-term offset variations.

Equations (16) and (17) can be used to compare offset accuracies between different spacecraft, despite them taking measurements in different environments, under different ambient conditions: (i) c may be computed for each spacecraft, smaller c indicating more accurate offsets, or (ii) c may be held constant, and offset uncertainties/deviations from different spacecraft may be compared to values of ΔO_f predicted by equations (16) and (17).

We choose option (ii) and compare the predictions by equations (16) and (17) with our results from the previous section (*THEMIS* case): There we obtained an offset vector from $N = 2511$ subintervals, yielding $\sum_i |\boldsymbol{B}_i^\mathrm{a}|/N = 16.82\,\mathrm{nT}$. Therewith, equations (16) and (17) predict: $\Delta O_\mathrm{f} = 2.2\,\mathrm{nT}$. As the actual deviation of $|\boldsymbol{O}_\mathrm{f}|$ (equation 14) from zero is 0.87 nT, the estimate ΔO_f has to be regarded as rather conservative. Also, the error estimates for $N = 500$ and 1000 subintervals, 3 and 2 nT, are lower than the corresponding ΔO_f estimates of 4.9 and 3.5 nT, when assuming $\sum_i |\boldsymbol{B}_i^\mathrm{a}|/N = 16.82\,\mathrm{nT}$.

5 APPLICATION TO *ROSETTA*

Finally, we apply the 3D mirror mode method to magnetic field data from the *Rosetta* Plasma Consortium magnetometer (RPC-MAG). The *Rosetta* mission of the European Space Agency (ESA) was designed to explore the nucleus and environment of comet 67P/Churyumov–Gerasimenko to which end it carries remote observation as well as *in situ* instruments (Glassmeier et al. 2007b). The main goal of the mission, pertaining to the plasma environment, was to explore the connection between the solar wind and the cometary ion environment. This means measuring the magnetic field and ion and electron densities, temperatures and energies. Due to mission requirements, the spacecraft is three-axis stabilized. The magnetometer is located on a boom at a distance of 1.5 m to the main spacecraft body to reduce the influence of magnetic fields generated by other instruments and electronics. This boom length is (much) lower than in the *THEMIS* and *Cassini* cases.

In addition, due to temperature and hysteresis effects, and due to a magnetically polluted spacecraft, there remains a highly variable offset vector of up to 30 nT in magnitude that needs to be determined and subtracted to facilitate the correct interpretation of the data. Methods using Alfvénic fluctuations in the IMF cannot be applied for the duration of the mission, because the magnetic field at a comet is significantly enhanced and modified by the incorporation of cometary ions into the solar wind flow (Biermann, Brosowski & Schmidt 1967; Nilsson et al. 2015; Goetz et al. 2017). Furthermore, *Rosetta* does not reach the unperturbed solar wind during the mission.

However, *Rosetta* entered the diamagnetic cavity on several occasions (Goetz et al. 2016a,b). Within the cavity, the magnetic field is practically absent (Neubauer et al. 1986; Cravens 1987). Furthermore, this region is characterized by very low levels of magnetic field fluctuations with respect to the plasma environment outside, making it easily discernible in the data even if the magnetic field is not zero due to an uncorrected offset. The residual magnetic field values in the cavity provide a good indication of the offset at the time of the cavity encounter, which may then be used to verify offsets determined by the 3D mirror mode method from data intervals adjacent to the cavity observations.

We apply the 3D mirror method to data obtained between 2015 July 6, 00:00 UT, and 2015 July 9, 24:00 UT (4 d). At this time, the spacecraft was located at a distance of about 200 km away from the cometary nucleus with a phase angle of 90° to the Sun-comet line. The chosen interval fulfils the following requirements: first, there are highly compressional waves present. Secondly, there are several short intervals during which *Rosetta* encountered the diamagnetic cavity. Thirdly, the magnetometer was operating with the highest sampling rate of 20 Hz.

Downloaded from https://academic.oup.com/mnras/article-abstract/469/Suppl_2/S675/4265357
by guest
on 13 November 2017

The first requirement is easily fulfilled by the presence of asymmetric structures with a large fluctuation amplitude $\Delta B/B \gg 1$. These structures appear in the plasma environment surrounding the diamagnetic cavity (Goetz et al. 2016a) and have the same characteristics in minimum/maximum variance analysis as mirror mode waves. Thus, they are suitable for the 3D mirror mode method. Although different kinds of mirror mode waves have also been found in the coma of comet 67P (Volwerk et al. 2016), they are not as ubiquitous as in the Earth's magnetosheath.

We require the second, because measurements in the diamagnetic cavity provide us with an opportunity to check the offsets calculated by the 3D mirror mode method: the offset-corrected fields inside the cavity should ideally vanish.

The last requirement arises from the fact that the magnetic field measurements are contaminated by the signatures of reaction wheels (Glassmeier et al. 2007a). This contamination can be and has been removed by low-pass filtering the high resolution data available in ESA's Planetary Science Archive (PSA) and resampling it to a 1 s resolution, which is sufficient for the 3D mirror mode method.

Finally, it is worth pointing out that during the 4 d selected for this test, the sensor was not greatly affected by temperature variations. Hence, the offsets can be regarded to be relatively constant, in comparison to other intervals.

The data used here are in instrument-fixed coordinates, to ensure that any spacecraft attitude adjustments are not translated into offset changes. In panel (a) of Fig. 6, the uncorrected magnetic field data are shown as measured by *Rosetta* during the four days of interest. It can be seen that large compressional waves are present, in particular, during the days 7–9 of July. In total, using $t_{\rm int} = 3$ min and $t_{\rm shift} = 10$ s, 33 030 subintervals of data without gaps are found, having excluded all cavity and cavity boundary intervals, as the highly compressional signals at the cavity edges would otherwise help in the offset determination process (Goetz et al. 2016a).

Panels (b) and (c) depict the magnetic field subinterval averages $\boldsymbol{B}^{\rm a}$ and the maximum variance directions $\boldsymbol{D}$, respectively. ΔB and ΔD are shown in panels (d) and (e) of Fig. 6, and also in Fig. 7. From this latter figure, it is apparent that the choice of $C_{\Delta B} = 10$ nT and $C_{\Delta D} = 20^\circ$ is appropriate for the considered *Rosetta* interval, as it is for the *THEMIS* case. In this case, however, even a smaller $C_{\Delta D}$ would be possible, as there are more subintervals featuring $\Delta D < 10^\circ$. By applying these two criteria, we are left with 7347 subintervals.

Again, we choose $C_\alpha = 30^\circ$ (see initial α values in panel f of Fig. 6), resulting in just 1063 subintervals being selected for the first iteration of the 3D mirror mode method (see panel g). Note that during the first few hours of July 6, no subintervals are selected. The reason is that the field is mainly directed along y (see green trace in panel b), but the maximum variance direction points along x (D_x depicted by the blue line in panel c reaching values close to 1 and -1). Hence, the fluctuations appear transversal and not compressional.

After 111 iterations, setting again $C_O = 10$ pT and $S = 10$, we obtain

$$\boldsymbol{O}_{\rm f} = (10.65,\ -13.27,\ 1.72)\,{\rm nT}. \qquad (18)$$

Over the iterations, the number of subintervals fulfilling $\alpha < C_\alpha$ increases to $N = 2289$.

Apparently, the offset vector is significantly different from zero, much more than in the *THEMIS* and *Cassini* cases. The reason is that the *Rosetta* data have been calibrated using only the calibration parameters determined on ground (Glassmeier et al. 2007a). *THEMIS* and *Cassini* data, instead, were calibrated in flight, i.e. calibration

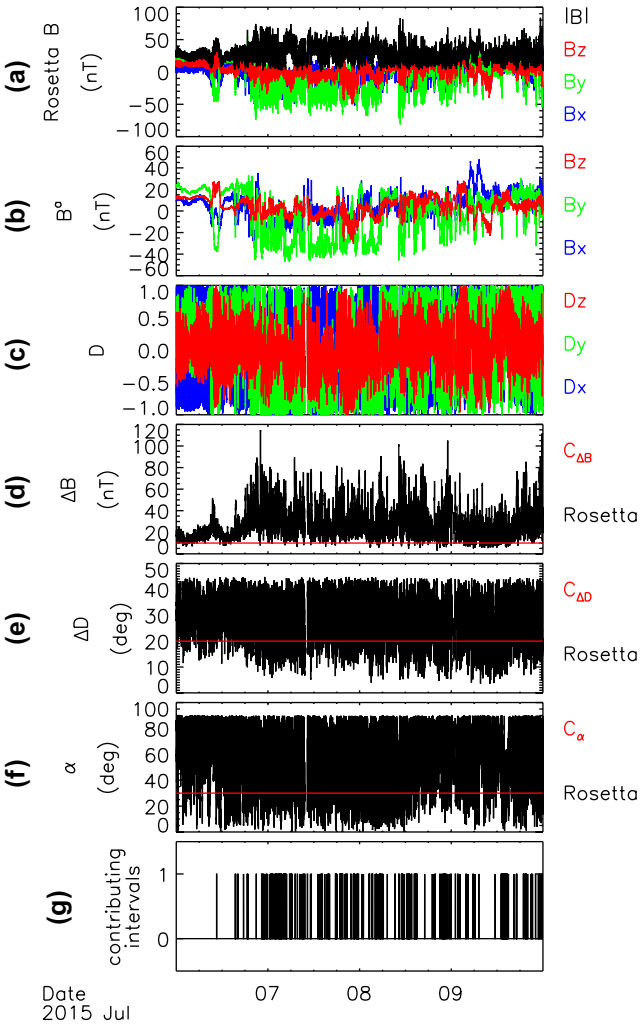


Figure 6. From the top to bottom: (a) original (not offset corrected) *Rosetta* magnetic field data $\boldsymbol{B}$ in instrument-fixed coordinates, (b) subinterval averages $\boldsymbol{B}^{\rm a}$, (c) maximum variance directions $\boldsymbol{D}$, (d) field changes in that direction ΔB (black) and $C_{\Delta B} = 10$ nT (red), (e) angular uncertainties ΔD with respect to $\boldsymbol{D}$ (black) and $C_{\Delta D} = 20^\circ$ (red), (f) angle between $\boldsymbol{D}$ and $\boldsymbol{B}^{\rm a}$ (black) and $C_\alpha = 30^\circ$ (red), and (g) a flag to identify the selected subintervals that fulfil all criteria and, hence, contribute to offset determination (first iteration).

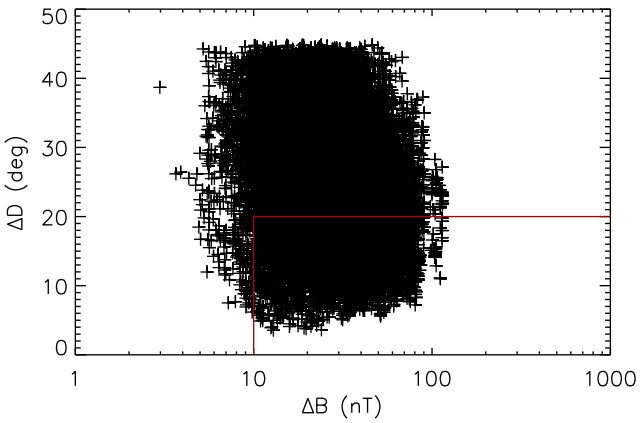


Figure 7. ΔD over ΔB pertaining to 33 030 subintervals of Rosetta data from 2015 July 6 to 9. The red lines depict the 10 nT and 20° levels, respectively.

Downloaded from https://academic.oup.com/mnras/article-abstract/469/Suppl_2/S675/4265357
by guest
on 13 November 2017

parameters were determined for and applied to the specific intervals considered in this study.

Goetz et al. (2016a) developed a temperature dependent offset model based on diamagnetic cavity observations, but this model has not been applied here to the *Rosetta* data, to avoid aiding the 3D mirror mode method. Nevertheless, we can use cavity observations to check if the offset in equation (18) is correct. From all cavity intervals within the 4 d of data considered, we obtain a mean offset vector of

$$\boldsymbol{O}_{\rm c} = (6.50,\ -12.81,\ 4.78)\,{\rm nT} \pm (5.86,\ 2.51,\ 2.70)\,{\rm nT}. \quad (19)$$

The uncertainties are the standard deviations of the magnetic field components within the cavity. Taking into account these uncertainties, only the z-component of $\boldsymbol{O}_{\rm f}$ (equation 18) has to be considered a bit too low, when assuming that the field should vanish within the cavity. The difference $\boldsymbol{O}_{\rm diff} = \boldsymbol{O}_{\rm f} - \boldsymbol{O}_{\rm c}$ yields

$$\boldsymbol{O}_{\rm diff} = (4.16,\ -0.47,\ -3.06)\,{\rm nT}. \quad (20)$$

The magnitude thereof is $|\boldsymbol{O}_{\rm diff}| = 5.18\,{\rm nT}$.

The corresponding mean of the magnetic field averages over the selected ($N = 2289$) subintervals is $\sum_i |\boldsymbol{B}_i^{\rm a}|/N = 22.47\,{\rm nT}$. Therewith, we obtain an estimate of the uncertainty via equations (16) and (17) of $\Delta O_{\rm f} = 3.09\,{\rm nT}$. Apparently, $|\boldsymbol{O}_{\rm diff}| = 5.18\,{\rm nT}$ is somewhat higher than predicted. However, the standard deviation of the cavity fields $|\Delta\boldsymbol{O}_{\rm c}| = 6.92\,{\rm nT}$ is even higher, which indicates fluctuations in the true offset on this order.

Goetz et al. (2016a) have modelled the dependence of the *Rosetta* magnetometer offsets on sensor temperature (see also Goetz et al. 2017). As mentioned above, we do not correct for this temperature dependence in the data. Hence, $\boldsymbol{O}_{\rm f}$ is associated with an average temperature over the subintervals considered for offset determination, while $\boldsymbol{O}_{\rm c}$ is associated with another average temperature over the cavity intervals. Slight differences between these two average temperatures explain part of the difference $\boldsymbol{O}_{\rm diff}$.

Furthermore, temperature variations within the cavity intervals account for one part of the large standard deviations in the cavity fields $\Delta\boldsymbol{O}_{\rm c}$. As Goetz et al. (2016a) found out, after applying their temperature dependent offset model, the cavity fields still fluctuate by up to 5 nT. Hence, another part of $\Delta\boldsymbol{O}_{\rm c}$ has to be attributed to offset variations that do not correlate with sensor temperature. Both temperature dependent and not temperature dependent offset variations (hence, a combination of instrument and spacecraft contributions to the offset) will contribute to $\Delta\boldsymbol{O}_{\rm c}$ and to a similarly large uncertainty in $\boldsymbol{O}_{\rm f}$, thus, making the relatively large difference $\boldsymbol{O}_{\rm diff}$ plausible.

Significant short term offset variations make the successful application of the 3D mirror mode method to *Rosetta* data more challenging, in comparison to the *THEMIS* or *Cassini* cases. Nevertheless, the offset result obtained constitutes a significant improvement, as documented in Fig. 8. The top panel shows the original magnetic field data. After excluding the cavity intervals (also the one observed around 10:00 UT on 2015 July 7), the method determines the offset given in equation (18). When subtracting this offset via equation (3), we obtain the corrected magnetic field measurements $\boldsymbol{B}_{\rm corr}$ shown in the bottom panel (c) of Fig. 8. As can be seen, the field is now much closer to zero within the cavity, as expected, although cavity intervals were not used in the offset computations.

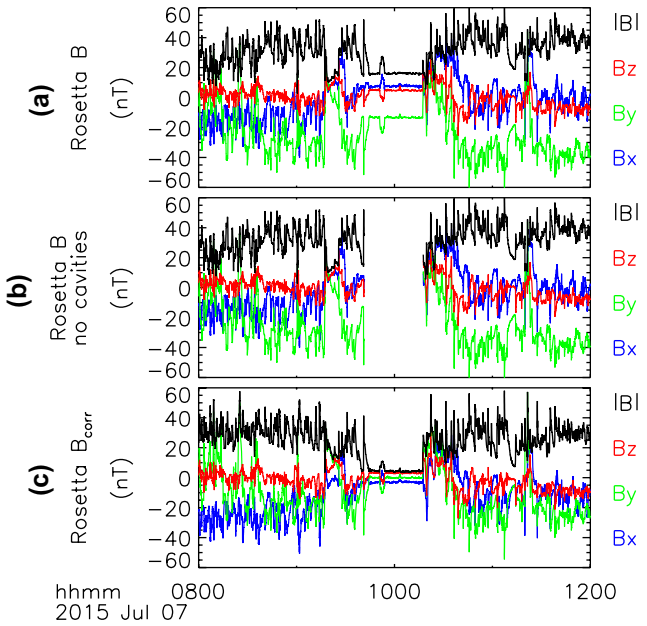


Figure 8. From the top to bottom: (a) original *Rosetta* magnetic field data $\boldsymbol{B}$ between 08:00 and 12:00 UT on 2015 July 7 in instrument-fixed coordinates, (b) same data without the cavity and cavity boundaries, and (c) with $\boldsymbol{O}_{\rm f}$ (equation 18) corrected magnetic field data $\boldsymbol{B}_{\rm corr}$.

6 CONCLUSIONS

In this paper, we introduce the 3D mirror mode method, which is able to determine fluxgate magnetometer 3D offset vectors from observations of highly compressional magnetic field fluctuations. We test the method by applying it to magnetic field measurements by: *THEMIS-C* in the subsolar terrestrial magnetosheath, *Cassini* in the dusk Jovian magnetosheath and *Rosetta* in the vicinity of comet 67P.

Based on over 2500 subintervals of compressional waves, extracted out of one month of *THEMIS-C* data, the 3D mirror mode method is able to achieve accuracies on the order of 1 nT or better. More/less subintervals result in more/less accurate offset results. Consequently, we find that accuracies better than 2 nT (3 nT) may be expected if more than 1000 (500) subintervals contribute, which is equivalent to 56 h (28 h) of terrestrial magnetosheath measurements.

It should be stressed that these results are valid for spacecraft with similar offset behaviour/stability and calibration accuracy to *THEMIS-C*, taking measurements in a similar environment to the terrestrial magnetosheath. Tests with *Cassini* and *Rosetta* data reveal that (in absolute terms) much better/worse offset accuracies may be achieved. In the *Cassini* case, the obtained offset is an order of magnitude more accurate (on the order of 0.1 nT), whereas in the *Rosetta* case, it is significantly less accurate (on the order of 5 nT). In particular, the test with *Cassini* data shows how important the average magnetic field strength is. In lower fields (i.e. in the Jovian magnetosheath), inaccuracies in the angle between the maximum variance and the mean magnetic field directions result in proportionally lower offset uncertainties.

This behaviour is expressed in equation (16), which allows us to compare the accuracies achievable by *THEMIS-C*, *Cassini* and *Rosetta* despite that fact that the numbers of contributing subintervals or the ambient magnetic field strengths are different. We find that *THEMIS-C* data yield the most accurate offsets, relatively. The reason is probably the spin-stabilization of the spacecraft. A dynamic spin plane offset correction implemented in the *THEMIS* calibration software adjusts the spin plane offset components over time. Hence, two out of three offsets are already 'perfectly'

Downloaded from https://academic.oup.com/mnras/article-abstract/469/Suppl_2/S675/4265357
by guest
on 13 November 2017

calibrated and stable. The stability of the third (spin axis) component is ensured by a relatively long boom and a magnetically clean *THEMIS-C* spacecraft. *Cassini* yields slightly less accurate offsets, relatively. Its offsets cannot be corrected dynamically, as *Cassini* is a three-axis stabilized spacecraft. Its very long boom, however, reduces the spacecraft influence on the magnetic field measurements, keeping offset variations small. *Rosetta* data yield the least accurate offsets, in relative and absolute terms. The reasons are variations in the offset on the order of several nanotesla over short time-scales, partly linked to sensor temperature variations, partly associated with changes in the magnetic field signature of the spacecraft.

Overall, we expect the 3D mirror mode method to be highly beneficial for the in-flight calibration of magnetometers on-board numerous past, present and future three-axis stabilized spacecraft that orbit Earth, other planets, their moons or comets. If the spacecraft (i) do not spend time regularly in the pristine solar wind, (ii) do not perform roll manoeuvres regularly, (iii) do not feature electron drift instruments or absolute magnetometers whose data can be used for cross-calibration, and (iv) do not regularly enter regions from which we know a-priori how large the field should be (e.g. diamagnetic cavities), then the 3D mirror mode method is currently the only known method that can be used to determine magnetometer offsets.

What is the best (i.e. most accurate) option for offset determination will be dependent on the magnetic field conditions along the spacecraft orbit and on the capabilities and limitations of the spacecraft. In general, more accurate offsets are determined under low magnetic field conditions, based on larger statistical sample sizes, if the magnetometer offsets stay constant. If a spacecraft spends equal amounts of time in the pristine solar wind and in the dayside magnetosheath, then methods based on the analysis of Alfvénic solar wind magnetic field fluctuations might yield more accurate results than the application of the mirror mode method, because the magnetic field strength is lower in the solar wind than in the magnetosheath. However, if a spacecraft spends significantly more time in the magnetosheath than in the solar wind, then better statistics might make offsets from the mirror mode method more accurate. If offsets are determined via cross-calibration with an electron drift instrument or an absolute magnetometer (if available), then the achievable accuracies will largely be dependent on the uncertainties of the reference measurements; again, better statistics (more measurements in low and stable ambient fields) help to increase the accuracy. Low and stable fields are also advantageous when using spacecraft rolls for offset determination. In order to determine a full offset vector, rolls have to be performed around at least two orthogonal axes. Variations in magnetic fields over the duration of a roll will limit the achievable accuracy of that method. If rolls can only be performed in high or quickly varying fields, then results from the mirror mode method (if applicable) may end up being more accurate, though, usually, a few rolls under stable conditions should be sufficient to obtain a good offset estimate. Diamagnetic cavity measurements are probably the most accurate references for offset determination in the *Rosetta* case, though, in general, this option will be restricted to spacecraft measurements in the close vicinity of cometary nuclei. Correspondingly, the offset model by Goetz et al. (2016a) should yield better results within the applicable temperature range, but the 3D mirror mode method may help extend that temperature range to values not measured by *Rosetta* inside the cometary diamagnetic cavity.

Finally, we would like to point out that the basis of our newly developed 3D mirror mode method is the knowledge of and the selection with respect to very specific polarization properties of the analysed magnetic field variations. In this respect, the 3D mirror mode method is similar to established methods for offset determination (e.g. Belcher 1973; Hedgecock 1975). However, while these latter methods use Alfvénic perturbations that are purely transverse to the background magnetic field, the mirror mode method is based on the compressible nature of the variations. More generalized methods are currently being developed that make use of cross-polarization and other specific wave activity properties.

ACKNOWLEDGEMENTS

The Rosetta Plasma Consortium Magnetometer (RPC-MAG) data are available through the Planetary Science Archive (PSA) of the European Space Agency (ESA) and the Planetary Data System (PDS) of the National Aeronautics and Space Administration (NASA). *Rosetta* is an ESA mission with contributions from its member states and from NASA.

The work on RPC-MAG and the *THEMIS* fluxgate magnetometer (FGM) was financially supported by the German Ministerium für Wirtschaft und Energie and the Deutsches Zentrum für Luft- und Raumfahrt under contract 50QP 1401 and under contracts 50QP 1401 and 50OC 0302. We are indebted to the whole of the Rosetta Mission Team, the Science Ground Segment (SGS) and the Rosetta Mission Operations Centre (RMOC) for their outstanding efforts in making this mission possible.

We acknowledge the *Cassini* magnetometer (MAG) operations team at Imperial College London who provided the *Cassini* MAG measurements used in this study.

Furthermore, we acknowledge NASA contract NAS5-02099 and V. Angelopoulos for use of data from the *THEMIS* Mission. Specifically, we acknowledge C. W. Carlson and J. P. McFadden for use of electrostatic analyzer data.

REFERENCES

Acuña M. H., 2002, Rev. Sci. Instrum., 73, 3717
Alconcel L. N. S., Fox P., Brown P., Oddy T. M., Lucek E. L., Carr C. M., 2014, Geosci. Instrum. Meth. Data Syst., 3, 95
André N., Erdös G., Dougherty M., 2002, Geophys. Res. Lett., 29, 41
Angelopoulos V., 2008, Space Sci. Rev., 141, 5
Auster H. U. et al., 2008, Space Sci. Rev., 141, 235
Balogh A. et al., 2001, Ann. Geophys., 19, 1207
Baumjohann W., Treumann R. A., Georgescu E., Haerendel G., Fornaçon K.-H., Auster U., 1999, Ann. Geophys., 17, 1528
Belcher J. W., 1973, J. Geophys. Res., 78, 6480
Biermann L., Brosowski B., Schmidt H. U., 1967, Sol. Phys., 1, 254
Constantinescu O. D., Glassmeier K.-H., Treumann R., Fornaçon K.-H., 2003, Geophys. Res. Lett., 30
Cravens T. E., 1987, Adv. Space Res., 7, 147
Dougherty M. K. et al., 2004, Space Sci. Rev., 114, 331
Enríquez-Rivera O., Blanco-Cano X., Russell C. T., Jian L. K., Luhmann J. G., Simunac K. D. C., Galvin A. B., 2013, J. Geophys. Res., 118, 17
Erdős G., Balogh A., 1996, J. Geophys. Res., 101, 1
Frühauff D., Plaschke F., Glassmeier K.-H., 2017, Ann. Geophys., 35, 117
Gary S. P., Fuselier S. A., Anderson B. J., 1993, J. Geophys. Res., 98, 1481
Georgescu E. H. et al., 2006, in Fletcher K., ed., ESA SP-598: Proc. Cluster and Double Star Symposium, 5th Anniversary of Cluster in Space. ESA, Noordwijk
Glassmeier K.-H., Motschmann U., Mazelle C., Neubauer F. M., Sauer K., Fuselier S. A., Acuna M. H., 1993, J. Geophys. Res., 98, 20
Glassmeier K.-H., Boehnhardt H., Koschny D., Kührt E., Richter I., 2007a, Space Sci. Rev., 128, 1
Glassmeier K.-H. et al., 2007b, Space Sci. Rev., 128, 649
Goetz C. et al., 2016a, MNRAS, 462, S459

Downloaded from https://academic.oup.com/mnras/article-abstract/469/Suppl_2/S675/4265357
by guest
on 13 November 2017

Goetz C. et al., 2016b, A&A, 588, A24
Goetz C., Volwerk M., Richter I., Glassmeier K. H., 2017, MNRAS, 469, S268
Hasegawa A., 1969, Phys. Fluids, 12, 2642
Hedgecock P. C., 1975, Space Sci. Instrum., 1, 83
Kepko E. L., Khurana K. K., Kivelson M. G., Elphic R. C., Russell C. T., 1996, IEEE Trans. Magn., 32, 377
King J. H., Papitashvili N. E., 2005, J. Geophys. Res., 110, A02104
Leinweber H. K., Russell C. T., Torkar K., Zhang T. L., Angelopoulos V., 2008, Meas. Sci. Technol., 19, 055104
Lucek E. A., Dunlop M. W., Balogh A., Cargill P., Baumjohann W., Georgescu E., Haerendel G., Fornaçon K.-H., 1999, Geophys. Res. Lett., 26, 2159
McFadden J. P. et al., 2008, Space Sci. Rev., 141, 277
Matson D. L., Spilker L. J., Lebreton J.-P., 2002, Space Sci. Rev., 104, 1
Nakamura R. et al., 2014, Geoscientific Instrum., Methods Data Syst., 3, 1
Neubauer F. M. et al., 1986, Nature, 321, 352
Nilsson H. et al., 2015, Science, 347, aaa0571
Plaschke F., Narita Y., 2016, Ann. Geophys., 34, 759
Plaschke F., Hietala H., Angelopoulos V., 2013, Ann. Geophys., 31, 1877
Plaschke F., Nakamura R., Leinweber H. K., Chutter M., Vaith H., Baumjohann W., Steller M., Magnes W., 2014, Meas. Sci. Technol., 25, 105008
Price C. P., Swift D. W., Lee L.-C., 1986, J. Geophys. Res., 91, 101
Russell C. T. et al., 2016, Space Sci. Rev., 199, 189
Schmid D., Volwerk M., Plaschke F., Vörös Z., Zhang T. L., Baumjohann W., Narita Y., 2014, Ann. Geophys., 32, 651
Schwartz S. J., Burgess D., Moses J. J., 1996, Ann. Geophys., 14, 1134
Sonnerup B. U. O., Cahill L. J., Jr, 1967, J. Geophys. Res., 72, 171
Southwood D. J., Kivelson M. G., 1993, J. Geophys. Res., 98, 9181
Torbert R. B. et al., 2016, Space Sci. Rev., 199, 283
Tsurutani B. T., Smith E. J., Anderson R. R., Ogilvie K. W., Scudder J. D., Baker D. N., Bame S. J., 1982, J. Geophys. Res., 87, 6060
Tsurutani B. T., Lakhina G. S., Verkhoglyadova O. P., Echer E., Guarnieri F. L., Narita Y., Constantinescu D. O., 2011, J. Geophys. Res., 116, A02103
Volwerk M. et al., 2016, Ann. Geophys., 34, 1

This paper has been typeset from a TEX/LATEX file prepared by the author.

Downloaded from https://academic.oup.com/mnras/article-abstract/469/Suppl_2/S675/4265357
by guest
on 13 November 2017